

# The Lives of High Redshift Mergers

Tom McCavana<sup>1\*</sup>, Miroslav Micic<sup>1,2</sup>, Geraint F. Lewis<sup>1</sup>, Manodeep Sinha<sup>3</sup>,  
Sanjib Sharma<sup>1</sup>, Kelly Holley-Bockelmann<sup>3</sup> and Joss Bland-Hawthorn<sup>1</sup>

<sup>1</sup>*Sydney Institute for Astronomy, School of Physics, A28, The University of Sydney, NSW 2006, Australia*

<sup>2</sup>*Astronomical Observatory Belgrade, Volgina 7, P.O.Box 74 11060 Belgrade, Serbia*

<sup>3</sup>*Department of Physics & Astronomy, Vanderbilt University, Nashville, TN, USA*

3 March 2013

## ABSTRACT

We present a comparative study of recent works on merger-timescales with dynamical friction and find a strong contrast between idealized/isolated mergers (Boylan-Kolchin et al. 2008) and mergers from a cosmological volume (Jiang et al. 2008). Our study measures the duration of mergers in a cosmological N-body simulation of dark matter, with emphasis on higher redshifts ( $z \leq 10$ ) and a lower mass range. In our analysis we consider and compare two merger definitions; tidal disruption and coalescence. We find that the merger-time formula proposed by Jiang et al. (2008) describes our results well and conclude that cosmologically motivated merger-time formulae provide a more versatile and statistically robust approximation for practical applications such as semi-analytic/hybrid models.

**Key words:** (cosmology:) dark matter, methods: n-body simulations, galaxies: evolution, galaxies: kinematics and dynamics

## 1 INTRODUCTION

Galaxy mergers are aided by dynamical friction, a process that extracts energy and angular momentum from the orbit of an incoming galaxy through a gravitational wake that acts as a drag force. Its theoretical conception (Chandrasekhar 1943) was based on a point mass traveling through an in-finite, uniform and non-self gravitating medium. With relatively few modifications to account for mass loss in the satellite galaxy, it is used to estimate the duration of galaxy mergers. As such it is a centrepiece of galaxy evolution; for example, in semi-analytical and hybrid models of galaxy evolution the accuracy of analytical merger-times is directly responsible for quantities such as stellar mass, gas available to the central black holes, the distribution of galaxy colour and morphology (e.g. Kauffmann et al. 1993; Volonteri et al. 2003; Croton et al. 2006; Micic et al. 2007; Somerville et al. 2008; Micic et al. 2011).

In current  $\Lambda$ CDM cosmology the first objects to form in the universe were made out of dark matter (Zwicky 1933; Rubin et al. 1980). Widely known as Dark Matter Halos (DMHs hereafter), their formation through violent collapse and relaxation results in a shallow inner density profile, with the remainder of accreted dark matter trailing behind in a steep outer slope (Ciardi & Ferrara 2005). The first galax-

ies, known as proto-galaxies, are born at the heart of these DMHs from gas that has been virialized, radiatively cooled and collapsed into a centrifugally supported disk. These proto-galaxies are the birth place of quasars and AGNs which later evolve into the spiral and elliptical galaxies observed today. As dark matter halos merge into larger structures so do the central proto-galaxies. This process (thought to be responsible for the AGN duty cycle) feeds the central AGN by providing a reservoir of gas which is then accreted onto the central massive black hole.

The dynamics of DMH mergers is described with reasonable success by a combination of gravitational free-fall, dynamical friction and tidal stripping. Chandrasekhar's dynamical friction has been analytically developed to predict the coalescence time for a circular orbit from some initial radius (Binney & Tremaine 1987). Most versions of the approximating formula follow the form:

$$T_{\text{merge}} = C_{df} \frac{(M_h/M_s)}{\ln \Lambda} \frac{f(\epsilon)r_*}{V_c(r_{vir})}, \quad (1)$$

where  $C_{df}$  is a constant,  $M_h$  and  $M_s$  are the masses of the host and satellite DMHs respectfully and  $f(\epsilon)$  is a function of circularity introduced analytically by Lacey & Cole (1993).  $\ln \Lambda$  is the Coulomb logarithm (discussed below),  $V_c(r_{vir})$  is the circular velocity at the virial radius ( $r_{vir}$ ) of the host halo, and  $r_*$  is a radius that varies depending on assumptions made. For bound circular orbits,  $r_*$  is the initial radius  $r_i$  (Binney & Tremaine 1987). In the more general case of a

\* E-mail: mccavana@physics.usyd.edu.au

bound orbit (radial or tangential)  $r_*$  is  $r_c(E)$  (Lacey & Cole 1993).  $r_c(E)$  is the radius that a circular orbit would have with the same orbital energy.  $r_*$  is also often approximated by  $r_{vir}$  as most works assume  $r_i \approx r_{vir}$  or  $r_c(E)/r_{vir} \approx 1$ .

Studies to improve the approximation of DMH merger-times (and by proxy the effects of dynamical friction) are numerous and range from analytical/semi-analytical (e.g. Weinberg 1989; Tremaine & Weinberg 1984; Lacey & Cole 1993; Benson et al. 2005; Taylor & Babul 2001; van den Bosch et al. 1999; Colpi et al. 1999) to numerical (e.g. Ahmad & Cohen 1973; Lin & Tremaine 1983; Tormen et al. 1998; Hashimoto et al. 2003; Fujii et al. 2006). Significant work has also been done to assess the accuracy of the Coulomb logarithm (see e.g. Jiang et al. 2008). Analytically,  $\Lambda$  is found to be a function of the maximum and minimum impact parameters. For extended bodies a better agreement is found with  $\ln \Lambda = \ln(1 + M_h/M_s)$ , where the satellite mass is determined at in-fall.

In order to refine the accuracy of dynamical friction formulae, Boylan-Kolchin et al. (2008, BK08 hereafter) explore merger timescales over a range of mass ratios, circularities and orbital energies using a suite of simulations of isolated mergers. In their analysis they build two well resolved Hernquist halos and merge them in various combinations of initial orbital parameters. They also explore the influence of baryons and find that including a stellar bulge ( $M_*/M_{DM} = 0.05$ ) shortens the merger-time by  $\approx 10\%$ . BK08 produce an empirical formula that relates merger-time to a mergers initial orbital parameters. They argue that a typical application of equation 1 systematically underestimates the merger-times seen in their simulation. This discrepancy grows as the host becomes larger than the satellite.

As one of the first simulations to study dynamical friction in a cosmological context, Jiang et al. (2008, J08 hereafter) developed a merger-time formula using direct measurements from a high resolution cosmological SPH/N-body simulation. Their measurements provide a more physically motivated approach for estimating merger-times. Galaxies merge in the astrophysically realistic context of cosmological structure formation. In their analysis they take the analytical formula of Lacey & Cole (1993) and break it down into its principle components, fitting each parameter in order of importance using their measurements of mergers between  $0 \leq z \leq 2$ . J08 find that using alternate forms of Coulombs logarithm gives a better agreement in the mass ratio dependence. They also propose a new form of the circularity dependence that better accounts for radial orbits (where the formerly used powerlaw breaks down). In contrast to Navarro et al. (1995), J08 find that the commonly used formula from Lacey & Cole (1993) systematically underestimates the merger-time for minor mergers and overestimates the merger-time for major mergers. They conclude their study by providing a statistically robust and cosmologically founded formula for merger-times. A follow up work Jiang et al. (2010) addresses minor issues in the baryonic physics such as overcooling.

In the current work we extend J08s study in two ways. Firstly by confirming their result using a different area of structural evolution, i.e. looking at higher redshifts ( $z \leq 10$ ) and a lower mass range. To this end we find our results are described well by J08s fitting formula. The second is by giving an independent comparison with BK08 who published

at around the same time. Both works look at the impact of orbital parameters on merger-timescales, however in very different ways. BK08 are able to make clean and accurate measurements as they are dealing with an isolated/closed system. J08 conversly, are looking at mergers amidst cosmological structure formation where kinematics can be affected by the local environment.

One difference between J08 and this study is the way in which merger-time is defined. We explore two types of merger; mergers that finish with coalescence of the two halo centres as well as mergers that are concluded by the tidal disruption of the satellite. These two merger criteria are explained in greater detail in the method.

It is necessary to highlight that the simulation used in this work contains dark matter only, while the study of J08 used a hydro/N-body simulation including gas and star formation. Using a dark matter only simulation has limitations. With regard to mergers defined by halo cores coalescing, it is assumed that galaxies lie in the centre of their dark matter halos and while this is a reasonable assumption it does not represent a 1-1 mapping when studying effects such as AGN activity and SMBH growth. With respect to the tidal disruption merger definition, the disruption of the dark matter halo does not necessarily correspond to tidal disruption of the galaxy. It is reasonable to assume that there is a connection between the two and at the very least the disruption of the DMH serves as proxy for the tidal stripping time of the galaxy.

The aim of this paper is to assess the validity of currently used merger-time formulae with as many mergers (of sufficient resolution) as possible. The focus is to better approximate the merger-times of DMHs in an astrophysically realistic context even if this does not correspond to an improvement in the description of dynamical friction in idealized isolated cases.

We describe our method in section 2, present the results of our comparison in section 3 followed by conclusions in section 4.

## 2 METHOD

We ran a cosmological N-body simulation using the code GADGET2 (Springel 2005). We then identify DMHs using P-groupfinder. For each halo at  $z=0$  we construct a merger-tree, which gives us a detailed dynamical history of all the halos in our simulation at all redshifts and allows us to look at all the mergers in the volume. Once mergers are identified we track them in subsequent snapshots on a particle by particle basis. In the following sub-sections we describe the details of the above steps.

### 2.1 Simulation and Group Finding

A cosmological N-body simulation of dark matter was used to simulate a volume of the universe,  $10 h^{-1} \text{Mpc}^3$  on one side, from redshift  $z=50$  to  $z=0$ . The relevant cosmological parameters were from WMAP3 data:  $\Omega_M=0.24$ ,  $\Omega_\Lambda=0.76$ ,  $\sigma_8=0.74$  and  $h=0.73$  (Spergel et al. 2007). Our mass resolution is  $4.9 \times 10^5 M_\odot h^{-1}$  (corresponding to  $512^3$  particles) and we saved 102 snapshots between redshifts  $z=19$  and  $z=0$ .

The initial conditions (ICs) at  $z=50$  were calculated

using the Zel'Dovich approximation, which assumes a linear evolution in density from  $z=1000$  to the starting redshift (Zel'Dovich 1970). It is true that using a higher starting redshift and more sophisticated methods of initializing the volume will result in a slightly different mass function (Crocce et al. 2006), we argue that this will not affect the measurement of merger-times for individual mergers. Analysis of  $512^3$  runs for 30 and  $100 h^{-1}\text{Mpc}^3$  volumes (with WMAP 5 and 7 year releases) is currently underway. The new volumes will be evolved from a redshift greater than 250 and will allow a much more detailed description of the merging populations.

We continue by identifying dark matter halos in a post simulation analysis with P-groupfinder using the Friends-Of-Friends (FOF) approach. We used the typical linking length of 0.2 times the mean inter-particle separation (corresponding to 3.9 kpc).

## 2.2 Merger-Tree

For every halo at  $z=0$  we created a merger-tree. Our merger-trees were constructed in the conventional fashion whereby we take a parent halo from snapshot  $i$  and look for its largest contributor in snapshot  $i-1$ . Halos are linked to their ancestors and descendants by unique particle ids. Some common pitfalls associated with building a merger-tree in this way are what we refer to as flybys and bridged halos. Flybys occur when the satellite halo enters the host halo only to continue on a perturbed (but ultimately unbound) trajectory in subsequent snapshots. Bridging happens when two small satellites appear to merge prior to falling into a much larger potential/halo. This is registered in the merger tree as two hierarchical mergers, but in reality the larger halo has simply accreted two small satellites.

Both of these problems arise from the discrete nature of simulations outputs. Addressing the impact of these systematic errors on galaxy evolution and black hole growth models (e.g. Volonteri et al. 2003; Somerville et al. 2008; Micic et al. 2007, 2011; Kauffmann et al. 1993; Croton et al. 2006) is beyond the scope of this paper, however further research on this topic is important to understand and quantify the consequences this will have on current models (Poole in prep, also see Sinha & Holley-Bockelmann 2012). In the appendix we discuss some of the steps taken in the construction of our merger-trees to avoid false or artificial mergers.

## 2.3 Halo Definitions and Merger-Tree Pruning

We track halos with at least 500 particles. While the FOF halo mass is used to discern relevant halos in the merger-tree, the virial mass and radius are used in all other calculations. We approximate the virial mass and radius by the spherically averaged over-density. We define a halo where  $\rho_{\text{vir}}(z) = 200 \rho_{\text{crit}}(z)$ , in which  $\rho_{\text{vir}}(z)$  is the average density within the virial radius and  $\rho_{\text{crit}}(z)$  is the critical density of the universe at the given redshift. Our merger-tree is constructed using halo masses defined by the FOF-groupfinding algorithm. After applying the SO algorithm to these halos we find several of them lack a significant over-density (that would be classified as a core). These halos are naturally excluded.

We calculate the centre of each halo potential using an iterative approach (e.g. Power et al. 2003). We calculate the centre of mass of the group and proceed to remove particles beyond  $0.98 r_i$ , where  $r_i$  is the current radius ( $r_0 = r_{\text{vir}}$ ). We then re-calculate the centre of mass for new set of particles and repeat the process until the number of particles reaches 5% of the original set. Halo velocities are approximated using the weighted mean, where weights are based on the distance from the centre of the potential.

We made several cuts to our collection of mergers in order to make our analysis set. As previously stated, there are a notable number of artificial mergers that we excluded from constructing our merger-tree. Flybys and bridged mergers have a significant impact on the accuracy of merger-trees, and we developed measures to exclude these from the analysis (see appendix). In general phase-space merger-tree codes (e.g. Behroozi et al. 2011) mitigate many of these artificial mergers automatically. Naturally we exclude any merger that does not finish by the end of our simulation. The effects of this can be seen as a distinctive curve in the upper left corner of the raw data plots of figure 1. This introduces a selection bias to our data set which will be discussed later.

## 2.4 Defining Merger-Time

Merger-time can be defined in multiple ways. Most involve the evolution of a characteristic or property of the merger such as separation, specific angular momentum or the number of bound particles, each has its own pitfall. Separation becomes an inaccurate proxy for highly radial orbits. Tidal disruption can impede the measurement of kinematics when using a specific angular momentum criteria. The number of bound particles is a relatively robust condition but is best tuned to track mergers that entirely disrupt the satellite. It is, however, highly dependent on the criteria for disruption and the force and mass resolution of the simulation (Klypin et al. 1999).

It is important that we clarify the definition of a merger in its astrophysical context. In this work we use two definitions of a merger, however we point the keen reader to Wetzel & White (2010)<sup>1</sup>. The types of merger assessed in this work are: (1) Coalescence, where halo cores (and their hosted galaxies) coalesce into a new potential before the satellite is tidally disrupted. This is the classically perceived picture of mergers in papers such as Tremaine et al. (1975) and White (1976). (2) Disruption, where the satellite is tidally disrupted before the halo cores coalesce. The various stellar streams in our own galaxy (Belokurov et al. 2006) are testament to the ability of tidal forces to disrupt satellites before they coalesce with their host.

The start of the merger is defined as the moment the satellite halo crosses the hosts virial radius. To get a better approximation of the exact moment we interpolate to

<sup>1</sup> Wetzel & White (2010) define 4 types of satellite removal which are directed toward the abundance matching approach to galaxy evolution. Semi-analytical and hybrid models should intrinsically incorporate their 3rd and 4th types of removal *if* flybys and bridged mergers are dealt with in an appropriate fashion by the merger-tree.

first order all merger properties between the adjacent snapshots. The end of the merger is quantified by two criteria: the evolution of specific angular momentum and the evolution of the number of bound particles. The Angular Momentum Criteria (AMC) is satisfied when specific angular momentum decreases to 5% of its initial value at the start of the merger. The angular momentum approach acts as a good criteria for coalescence and is the same approach taken by BK08. J08s halos have a baryons which can be used to directly track exactly when the two galaxies collide. The Bound Particle Criteria (BPC hereafter) covers tidal disruption. Similarly, the BPC is satisfied when the number of bound particles decreases to 5% of the initial value. We incorporate both types in a mixed definition, whereby the end of the merger is marked by whichever of the two criteria is satisfied first. When we compare our work to the literature we take care to note and match the merger criteria.

## 2.5 Tracking Mergers

We follow a fixed set of particles for the host and satellite halos at the time of in-fall. For the satellite we continue to use the same set of particles and retrieve their updated positions and velocities in subsequent snapshots. For the host, in order to take into account accretion, we use the original set of particles to track the central position and velocity of the halo but re-calculate the mass and radius based on the SO algorithm for all surrounding particles.

This approach eliminates errors typically associated with tracking halos using group-finders. One such error occurs when two over-densities of comparable size occupy the same FOF halo. Then the group-finder tracks the largest of the two as the main halo, but when the over-densities are of comparable size the tag can artificially switch to the other halo in the next snapshot (see Wetzel & White 2010). Another problem intrinsic to some subhalo finders (and any technique that relies on a density contrast to track substructure) is that they can intermittently lose substructure when it passes by the dense centre of the host (see Ludlow et al. 2009). The appendix highlights the benefit of using a fixed particle set to track mergers.

## 3 RESULTS

Throughout the results section we compare the different types of end-of-merger criteria and how they vary with orbital parameters. Recall that in both the AMC and BPC criteria the merger is considered complete when the value is 5% of its original value at in-fall. When we use AMC only, our data set consists of 1116 mergers (denoted by red unless stated otherwise). When BPC is applied the data set consists of 1199 mergers (blue). In the mixed set the end of the merger is defined by whichever criterion is satisfied first. This gives us 1438 mergers (black). Interestingly, 877 of the mergers have end-time measurements for both AMC and BPC methods. Furthermore, 55% of this sub-set have  $T_{BPC} < T_{AMC}$ . Throughout the results section any data bin used to compare variables contains a minimum of 40 mergers. The only bins that do not have  $N \geq 40$  are distribution functions, usually in the bottom panels. Overall we find that merger-time is most strongly correlated with the

dynamical timescale of the host halo. With regard to other merger parameters we get varied results for the different merger definitions.

The results are presented in the following form; in section 3.1 we look at the merger-time vs dynamical time relation, in section 3.2 we investigate mass ratio, circularity and orbital energy and finally in section 3.3 we compare our measured merger-times with the predictions of other merger-time formulae and provide our own best fit parameters.

### 3.1 Merger-Time with Redshift

Merger-times for such high redshift halos has remained unexplored in cosmological simulations. Figure 1 shows the measured merger-time as a function of the redshift at which the merger starts. The left panel shows data from the AMC and BPC merger sets separately. The central panel shows the mixed data set while the right panel shows the binned equivalent of each merger set. Bins are spaced equally in starting redshift. Points represent the bin median and error bars show the inter-quartile range. The red curve shows the limit of our measurements imposed by the end of the simulation at redshift  $z=0$  (if the merger does not end in Hubble time, it is excluded from the data set). The measurement limits introduced by the end of the simulation will give rise to a selection bias for our low redshift mergers. This can be seen in the first couple of bins in the right panel in figure 1 as data starts to deviate from the fit. In general, all three sets of data show that high redshift mergers take considerably less time to finish than those at low redshift.

One of the principal components of most prescriptions of merger-time is the dynamical timescale of the host halo  $T_{dyn}$ . In the context of halo mergers, dynamical time is the time necessary for a satellite halo to make its first pericentric passage of the host halo. The redshift evolution of a halos dynamical timescale in spherical collapse models can take multiple forms,

$$T_{dyn} = \frac{r_{vir}}{V_c(r_{vir})} = 0.1H(z)^{-1}. \quad (2)$$

where  $H(z)$  is Hubble's parameter and for the relevant cosmology is given by  $H^2(z) = H_0^2(\Omega_\Lambda + \Omega_m a^3)$ . Note we leave out a factor of  $\sqrt{2}$  in equation 2 as this will later be absorbed in other constants. The growth of a halos mass with redshift enlarges the virial radius as well as increases the dynamical time. Both BK08 and J08 take this effect into account. BK08 fit their orbital parameters to  $T_{merge}/T_{dyn}$  (where  $T_{dyn}$  is constant for their host) while J08 have a unique  $r_{vir}/V_c$  for each merger. The right panel in figure 1 shows how the merger-times measured in our simulation correlate with dynamical time. We plot 3 multiples of  $T_{merge} = \alpha T_{dyn}$  to illustrate the impact of  $T_{dyn}$  in our results. We do see indications that there is a redshift dependence beyond the  $T_{dyn}$  correlation. Such a dependence might manifest in the redshift evolution of the distribution of orbital parameters (like Wetzel 2011). We hope to study this in greater detail with the new simulations.

### 3.2 Other Orbital Parameters

The dependence of DMH merger-times is often tied to other orbital parameters such as mass ratio, circularity of the orbit

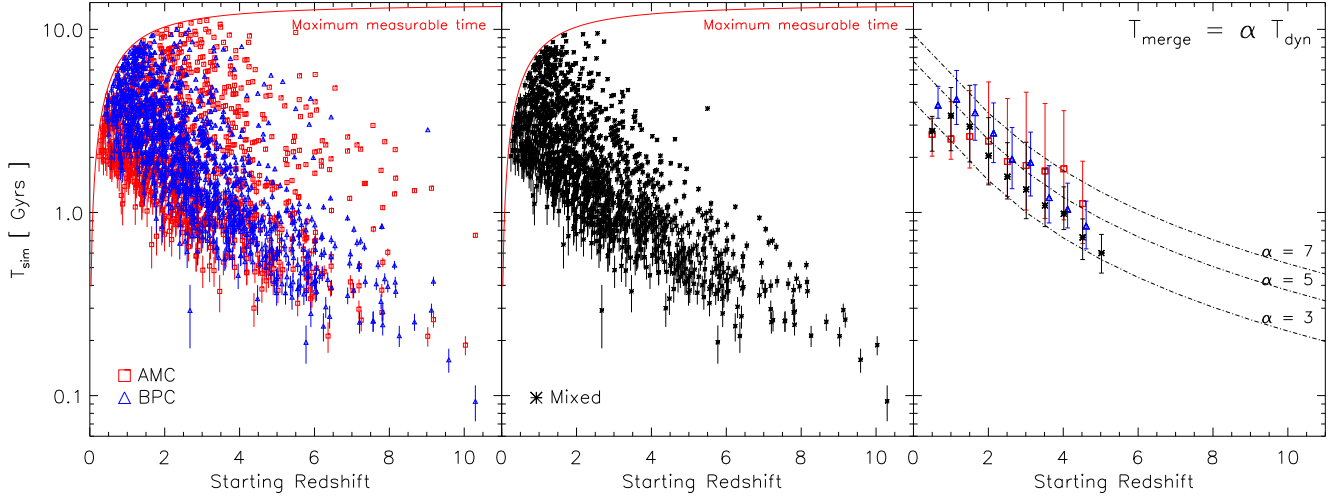


**Figure 1.** Merger-time against starting redshift. The plot holds a total 1438 mergers with a mixed end definition (threshold 0.05). The left panel shows the measurements for the AMC and BPC merger sets along with the associated errors. The middle panel shows the data for the mixed merger definition. The red curve for the first two panels represents the maximum merger-time measurable at a given starting redshift. The plot on the right shows the data for all sets binned in starting redshift. The central point for each bin corresponds to the median while error bars represent the interquartile range.

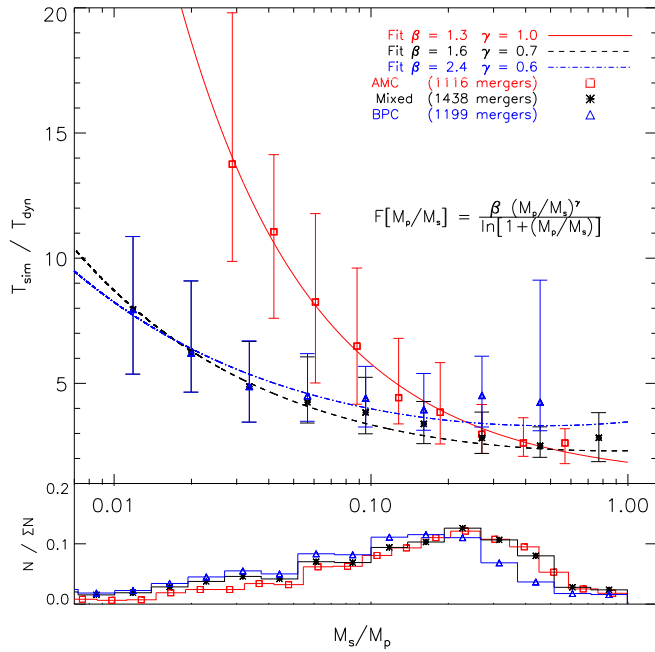


**Figure 2.** A comparison of  $T_{\text{merge}}/T_{\text{dyn}}$  vs mass ratio for the different end criteria. The central point in each bin represents the median while error bars correspond to the interquartile range. Each set is fitted to the equation shown. The bottom panel shows the fractional distribution of the merger sets with respect to mass ratio. The  $\chi^2$  fit values are shown in the top right.

and the orbital energy. In this section we explore these parameters and their dependence on the length of the merger.

Theory, especially with respect to the classically per-

ceived picture of mergers, expects a rather strong dependence of merger-time on mass ratio. There have been a number of works aiming to refine the form of the Coulomb logarithm. It is becoming increasingly accepted that the mass ratio dependence of merger-time is best characterized by:

$$T_{\text{merge}} \propto \frac{M_p/M_s}{\ln(1 + M_p/M_s)}, \quad (3)$$

where the Coulomb logarithm is  $\ln(1 + M_p/M_s)$ . Figure 2 shows measured merger-time (corrected for the  $T_{\text{dyn}}$  dependence we see in figure 1) as a function of the mass ratio of merging halos. In all sets of data there is a clear trend that the duration of the merger increases as the host halo becomes larger than the satellite. Our results for the AMC mergers are consistent with previous works (Wetzel & White 2010). While there is considerable scatter, the median value for each bin is in good agreement with the fit. The general scatter can be attributed to freedom in other orbital parameters. Despite fitting to the functional from BK08 (shown in figure 2) we find an exact match with J08, i.e that  $\gamma = 1.0$ .

When the BPC is used, we see that merger-time does not vary with mass ratio as expected. While the trend is correct, the dependence is weaker than seen in other works. The histogram in the bottom panel of figure 2 shows the fractional distribution of merger sets with respect to mass ratio.

In any closed two body system the exact trajectory can be described by circularity<sup>2</sup> and orbital energy. Both of these variables are hard to constrain in such a broad parameter space. As seen in J08 it is sometimes easier to look at weaker dependences by plotting them against  $T_{\text{sim}}/T_{\text{model}}$ .

<sup>2</sup> Circularity ( $\epsilon$ ) is related to the eccentricity( $e$ ) by  $\epsilon = \sqrt{1 - e^2}$ .

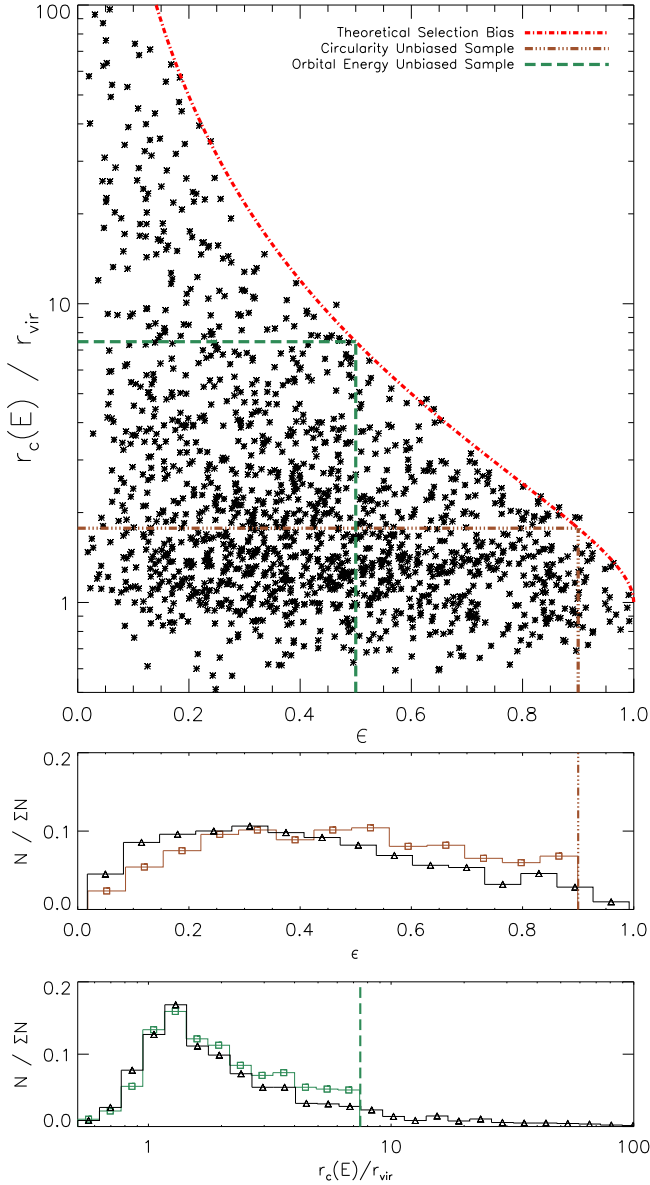


**Figure 3.** Circularity as a function of orbital energy. The top panel shows raw data with the selection bias (see text) marked by the red line. Also shown in the top panel is the unbiased samples used for the frequency distributions in the lower two panels.

Figure 3 shows orbital energy as a function of circularity for all mergers used in our analysis (i.e the mixed set). A selection bias can be seen in the top panel in the form of an ‘envelope’ of points. This is the product of the definition of merger start time (i.e the point at which the satellite crosses the hosts  $r_{\text{vir}}$ ). The detection of mergers with higher orbital energies and/or more circular orbits is limited by  $r_{\text{per}}/r_{\text{vir}} \leq 1$ ; in other words we will only detect mergers with orbital pericentres inside the hosts virial radius. An orbits pericentre is defined as  $r_{\text{per}} = a(1 - e)$ . For circular orbits the semi-major axis  $a$  is equal to  $r_c$ . This constraint can be expressed in terms of the circularity of the orbit such that

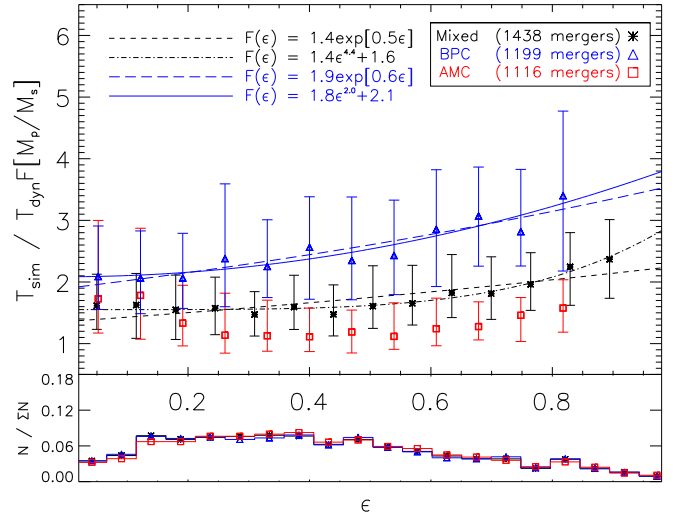


**Figure 4.** Merger-time as a function of circularity. Points correspond to the median while errors represent the interquartile range. The bottom panel shows the fractional distribution of the merger sets with respect to circularity.  $\chi^2$  fits are shown for the bound and mixed particle sets.

$$\frac{r_{\text{per}}}{r_{\text{vir}}} = \frac{r_c(1 - e)}{r_{\text{vir}}} \leq 1. \quad (4)$$

In the limit of this constraint  $r_{\text{per}}/r_{\text{vir}} = 1$ , equation 4 can be re-arranged to give,

$$\frac{r_c}{r_{\text{vir}}} = \frac{1 + \sqrt{1 - \epsilon^2}}{\epsilon^2}. \quad (5)$$

Equation 5 is shown in figure 3 as a red curve. It is in excellent agreement with the envelope.

The bottom two panels of figure 3 show the distribution of circularity and orbital energy respectively. In each panel we show the distribution of the full data set as well as an unbiased sample. Sub-samples are set by equation 5 and highlighted with lined boundaries in the top panel. The middle panel shows that selection bias has a strong influence on the distribution of circularities. This bias will not influence the fit of merger-time (section 3.3) but may have an impact on the fitting of circularity in figure 4. The unbiased set is in good agreement with Wetzel (2011) and Benson (2005).

The dependence of merger-time on circularity is less constrained than the mass ratio relation. Figure 4 shows merger-time against circularity for all 3 merger sets, corrected for the already fitted parameters. The overall trend shows that the duration of mergers increases with increasing circularity.

This positive correlation of merger-time and circularity is seen most strongly in the BPC set. Under the BPC definition, the trend corresponds to radial orbits tidally disrupting faster than circular orbits. This is expected as radial orbits make close central passages where tidal forces are strongest. The AMC merger set deviates from the trend significantly for more radial orbits. This deviation persists when an unbiased sample of circularities is used<sup>3</sup>. It appears to be physical

<sup>3</sup> It also persists under the condition that the satellite has a well resolved core.

and not an artifact of method or numerics. The implication for merger models is that, for well resolved satellites, both highly radial and highly circular orbits take a similar time to coalesce. Arguably, the binned points in figure 9 of J08 show a similar trend. Their trend is much weaker and it would require a detailed analysis to confirm it is a physical effect. Radial orbits  $\epsilon < 0.3$  are often overlooked in studies of this type, so perhaps this effect has not been appreciated.

We fit the mixed and BPC merger sets to the dependences seen in J08 and BK08 (shown top left). J08 have retained the analytically founded form<sup>4</sup> seen in Lacey & Cole (1993) while BK08 use an empirically motivated exponent. While both forms of the dependence are in accord with the data, the model with an extra fitting parameter (J08) shows a tighter agreement. We are not able to fit the AMC merger set due to the upward trend at low circularities. The bottom panel of figure 4 shows the frequency distribution of each set.

The final theoretical dependence is the orbital energy of the merger. As previously stated the proxy for the energy of the orbit is  $r_c(E)/r_{\text{vir}}$ . This compares the radius of a circular orbit (with the same energy as the orbit in question) with the virial radius of the host. The top panel of figure 5 compares the dependence of  $r_c(E)/r_{\text{vir}}$  with merger-time. Similar to previous figures, other dependencies on merger-time have been taken out. The exception is the circularity dependence for the AMC set. Overall there is a weak dependence in all 3 data sets. Other works suggest  $T_{\text{merge}} \propto [r_c(E)/r_{\text{vir}}]^\mu$ , where  $\mu \geq 1$ . BK08 find  $\mu = 1$ . J08 do not include an orbital energy dependence in their equation 5 for simplicity and ease of use. They do however propose an alternate form of the equation in the conclusion that incorporates the satellites orbital energy. We find a relatively consistent value of  $\mu = 0.1$  across all data sets.

The fractional distribution of  $r_c(E)/r_{\text{vir}}$  is displayed in a histogram in the lower panel. The range of  $r_c(E)/r_{\text{vir}}$  found in our simulation extends beyond the typically shown range. The peak of the distribution is slightly beyond 1. A close examination (snapshot to snapshot) of these extremely energetic orbits usually shows a close passing of a third body also orbiting host halo (a relatively common occurrence e.g. Sales et al. 2007).

### 3.3 Comparison with previous works

In this section we compare our measurements with the empirically derived formulae of Boylan-Kolchin et al. (2008) and Jiang et al. (2008). We remind the reader that the comparison is only with measurements from the AMC merger set as this is the merger definition under which their formulae were constructed. The best way to make this comparison is to look at the variance of the ratio of measured/predicted merger-time ( $T_{\text{sim}}/T_{\text{model}}$ ) for different orbital properties. The formulas used in our comparison are

Boylan-Kolchin et al. (2008):

$$T_{\text{merge}} = t_{\text{dyn}} \frac{A(M_h/M_s)^B}{\ln(1 + M_h/M_s)} \exp \left[ C \frac{J}{J_c(E)} \right] \left[ \frac{r_c(E)}{r_{\text{vir}}} \right]^D, \quad (6)$$

<sup>4</sup> Introducing an additional fitting parameter to accommodate the power law for highly radial orbits.

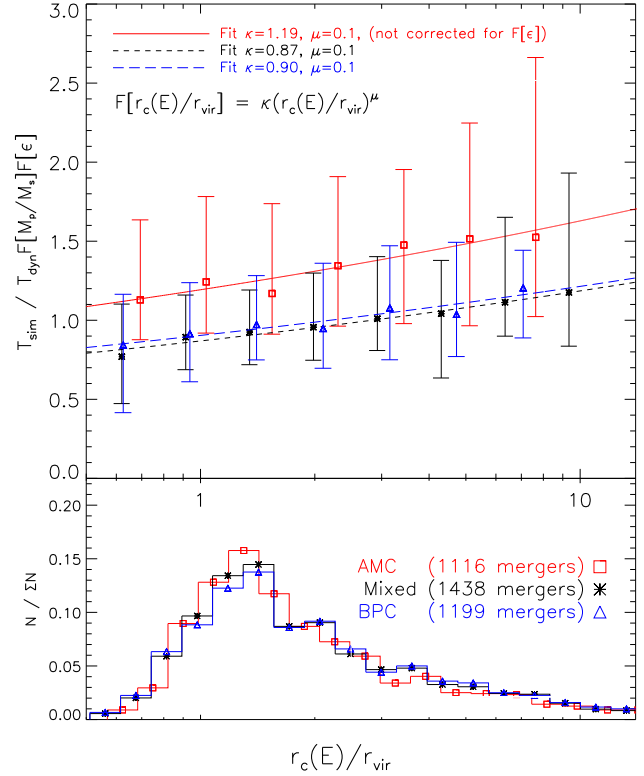


**Figure 5.** The top panel shows merger-time against  $r_c(E)/r_{\text{vir}}$  (a proxy for orbital energy). The bins are spaced equally in log. The distribution is skewed towards lower ratios, as shown in the lower panel. The  $\chi^2$  fitted parameters are shown top left. Points correspond to the median while errors show the interquartile range.

where  $J/J_c(E) \equiv \epsilon$  and their fitted constants are

$$A = 0.216, \quad B = 1.3, \quad C = 1.9, \quad D = 1.0. \quad (7)$$

Jiang et al. (2008):

$$T_{\text{merge}} = \frac{f(\epsilon) M_h}{2 C M_s \ln \Lambda} \frac{r_{\text{vir}}}{V_c(vir)} \quad (8)$$

where  $f(\epsilon)$  and  $\ln \Lambda$  are the corresponding fitted values from their work<sup>5</sup>, i.e  $f(\epsilon) = 0.94\epsilon^{0.6} + 0.60$  and our eq 3.

In addition to the above formulae, we do a maximum likelihood estimate of equation 6 using our merger-time measurements and find the following values.

$$A = 0.9, \quad B = 1.0, \quad C = 0.6, \quad D = 0.1. \quad (9)$$

We use these parameters to compare our fit with the other two works in figure 6. It shows the variance in  $T_{\text{sim}}/T_{\text{model}}$  with mass ratio, circularity and orbital energy. From top to bottom, figure 6 shows a comparison of BK08, J08 and the fitted values in this work. BK08 formalism deviates from our measurements as a function of mass ratio and orbital energy. At high host-to-satellite mass ratios BK08 overestimate the merger-time by a factor of  $\sim 3$ . The power law in the mass ratio dependence of BK08 is responsible for the deviation.

<sup>5</sup> We also compare with the alternate form of their fit (their equation 8) but find it to be a worse fit.



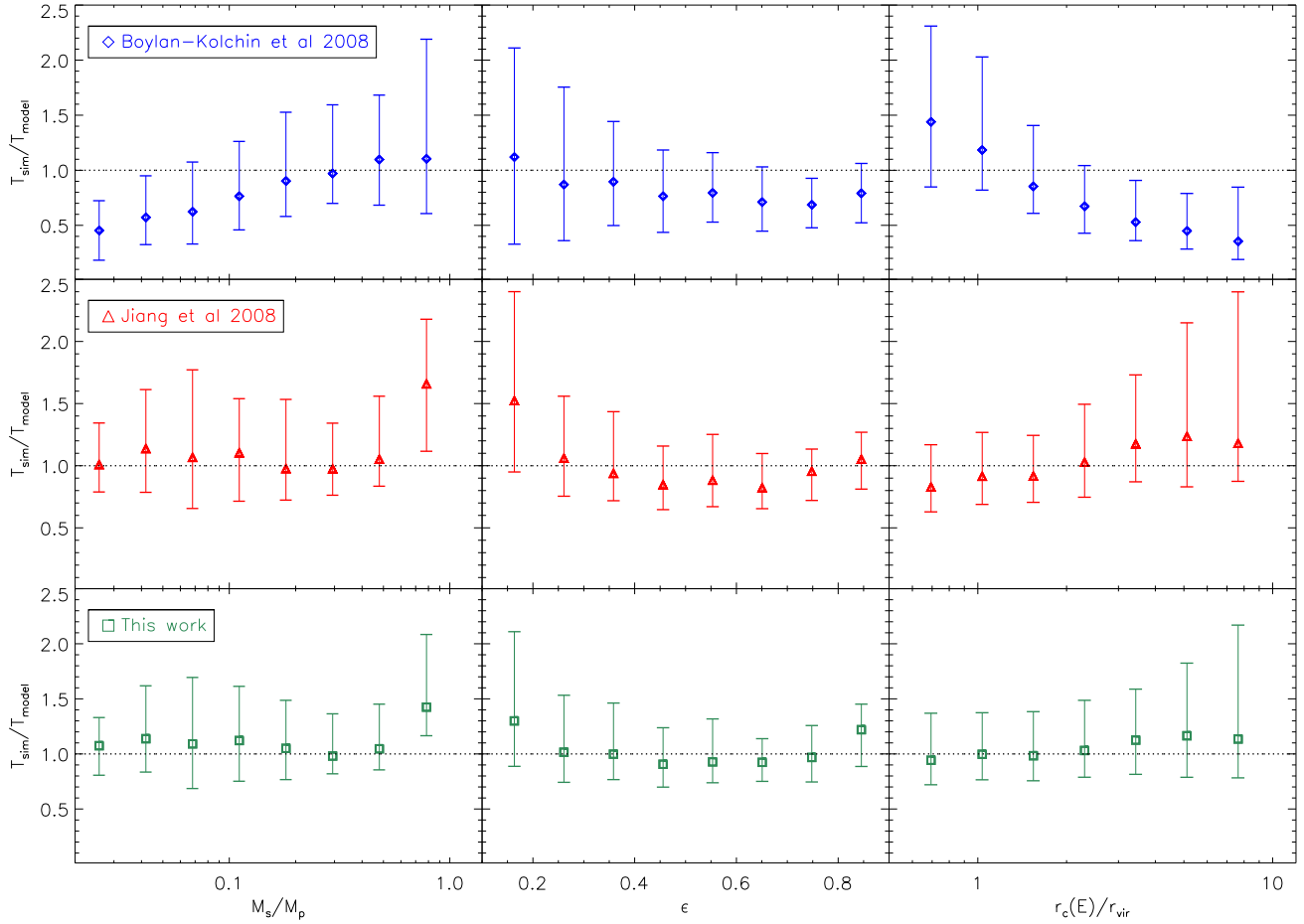


**Figure 6.**  $T_{\text{sim}}/T_{\text{model}}$  against mass ratio, circularity and orbital energy. In this plot we compare the empirically derived formulae of BK08 and J08 to the parameters found in this work. Points correspond to the median while errors show the interquartile range.

The discrepancy between BK08 and our fitted parameters (eq 7 and 9) indicates that the dependence of merger-time on circularity and orbital energy is weaker than previously derived. This illustrates the difference between an idealized isolated merger simulation and a full cosmological simulation. BK08s mergers were in isolation and had relaxed Hernquist halos. Conversely, the mergers in this work are in a cosmological context, here the host is still collapsing, undergoing multiple mergers at once and at the mercy of the tidal fields in its local environment.

BK08 explicitly state the range of validity of their formula as  $0.025 \leq M_s/M_p \leq 0.3$ ,  $0.3 \leq \epsilon \leq 1$  and  $0.65 \leq r_c(E)/r_{\text{vir}} \leq 1$ . We find that the range of valid orbital parameters corresponds to a significantly limited range of mergers in our simulation. A comparison within this parameter space can be seen in figure 7. It shows a very modest number ( $\approx 3\%$  of our AMC set) of comparable mergers.

The comparison to J08 produces a much tighter agreement in all three parameters (figure 6, middle panels). Maximum deviation occurs for equal mass ratio mergers as well as highly radial and energetic orbits. Our own fit to BK08s functional form shows a slight reduction in scatter when

compared with J08. This may just correspond to the different ways the mergers are qualified. Explicitly that we use specific angular momentum while J08 are able to measure when the baryons in the galaxies collide. Either way the results are very well described by the formula of J08.

As a note, caution should be taken when applying merger-time formulae. The accuracy of a formula can be highly dependent on the conditions under which it was derived. For example, as the merger progresses from some fiducial starting point the parameters of the merger change. The mass of the satellite typically decreases while the mass of the host increases.  $r_c(E)/r_{\text{vir}}$  tends toward zero, due to the growth of the virial radius with cosmic expansion as well as the dissipation of orbital energy from particle-particle interactions. These inputs will also vary depending on the halo finder/halo definition used to construct the merger-tree. The application of any approximating merger-time formalism should be consistent with the circumstances under which it was derived.



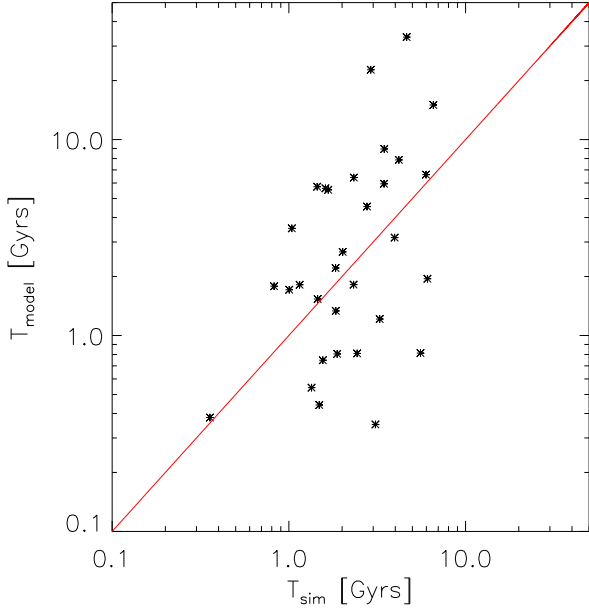


**Figure 7.** A comparison with BK08 showing the predicted and measured merger-times for mergers within their valid parameter range.

#### 4 CONCLUSIONS

This paper presents results of a cosmological N-body simulation in a small cosmological volume where dominantly spiral and dwarf galaxies form. We studied the mergers of the dark matter counterparts at high redshift. The mass and redshift range of our simulation has never been probed for merger-times. Our study considers two merger definitions that qualify the end of the merger, tidal disruption and core coalescence. We compare the measured merger-times from our simulation with the predicted times from other works.

The merger-times of DMHs is strongly dependent on the redshift at which the merger starts. This manifests itself in the redshift evolution of the host halos dynamical timescale. The dynamical timescale of a halo corresponds (approximately) to the time it takes for a point mass to make its first pericentric passage.

We consider both the AMC and BPC merger definitions (see section 2.5) in our analysis. Both scenarios impact on satellite removal in N-body/semi-analytic recipes of galaxy evolution. From the mergers that have both AMC and BPC end measurements, we find that 55% have  $T_{\text{BPC}} < T_{\text{AMC}}$ . We also find a selection bias that arises from the prerequisite that mergers included in our analysis must have  $r_{\text{per}}/r_{\text{vir}} \leq 1$ . This bias is characterized by equation 5 and should be considered in kinematic works of this type.

In the classical merger definition (AMC - where resolved satellites coalesce) we find good agreement with  $T_{\text{dyn}}$  and mass ratio relations. The circularity and orbital energy have less of an impact on merger-time. Our results show a much weaker dependence on orbital energy than analytical/ideal works. We find an interesting result with regard to the circularity dependence; for well resolved halos, highly radial and highly circular orbits finish in comparable time. This

low circularity region ( $\epsilon < 0.3$ ) is seldom probed, so it is possible (although unlikely) that this effect has been overlooked. BK08 do not cover  $\epsilon < 0.3$  in their study and J08 do not show as strong an upward trend for low circularities. We have taken steps to check for numerical and method based artifacts and plan to perform a more in-depth analysis in the future. For  $\epsilon > 0.3$  we find reasonable agreement with other works.

Our results according to the tidal-disruption merger-criteria (BPC) show some interesting variations. We found a tight correlation with the dynamical timescale of the host halo. We also see a dependence on mass ratio, although it is weaker than expected (see figure 3). Circularity for the BPC set shows shorter mergers have more radial orbits. In such orbits the satellite is exposed to stronger tidal forces.

We compare our measured merger-times with Boylan-Kolchin et al. (2008) and Jiang et al. (2008). We find a systematic deviation between our measurements and the predicted times of BK08 who numerically fit their formula from isolated mergers. By fitting our cosmological mergers to BK08s formula (eq 9) we are able to directly compare idealized and cosmological merger-times. As such, we find the biggest difference is the dependence on orbital energy ( $r_c/r_{\text{vir}}$  has a power of 0.1 instead of 1). Our results also show a mass ratio power of 1.0 (formerly 1.3) and a milder circularity dependence. We cannot say exactly why there is such a contrast between mergers in a cosmological context and those in isolation, however part of this discrepancy can be attributed to the fact that in cosmological structure formation multiple mergers occur simultaneously. In this work we have empirically found the differences between the two cases and the next step is to understand the physical mechanisms responsible.

In contrast to BK08, our data is well described by J08s approximating formula. Their empirically fitted formula was derived under the same cosmological N-body environment as this work. The differences between the simulations in J08 and this work are the inclusion of baryons as well as the mass and redshift range covered. We remind the reader that there are limitations to approximating the AMC and BPC merger measurements using dark matter alone. A comparison of our fit with J08 shows a slight reduction in scatter, however this is consistent with the different approaches used to measure merger-time. While both formulas fit the data well, the formula of J08 has one less input parameter which makes it easier to use. Our fit to BK08s form provides slightly reduced scatter at the expense of a additional parameter.

A comparison of the two works (isolated to cosmological) illustrates that while isolated/idealized numerical experiments are important to understand the underlying physics, a more versatile (statistically robust) approximation may serve better in non-ideal applications, i.e. semi-analytic/hybrid models.

#### 5 ACKNOWLEDGMENTS

The authors would like to thank Doug Lin, John Magorrian, Andrew Wetzel, Michael Boylan-Kolchin, Chunyun Jiang and Greg Poole for helpful discussion and correspondence. We would also like to thank the referee for fast and helpful feedback. GFL thanks the Australian Research Council for

support through his Future Fellowship (FT100100268) and Discovery Project (DP110100678). TM would like to thank the School of Physics, University of Sydney for support from the Denison Post-Graduate Conversion Award.

## REFERENCES

- Ahmad, A. Cohen, L. 1973, *ApJ*, 179, 885
- Behroozi, P. S., Wechsler, R. H., Wu, H.-Y. 2011, *ArXiv e-prints*: 1110.4372
- Belokurov, V., et al. 2006, *ApJ*, 642, L137
- Benson, A. J. 2005, *MNRAS*, 358, 551
- Benson, A. J., Kamionkowski, M., Hassani, S. H. 2005, *MNRAS*, 357, 847
- Binney, J. Tremaine, S. 1987, *Galactic dynamics*, ed. Binney, J. & Tremaine, S.
- Boylan-Kolchin, M., Ma, C.-P., Quataert, E. 2008, *MNRAS*, 383, 93
- Boylan-Kolchin, M., Springel, V., White, S. D. M., Jenkins, A., Lemson, G. 2009, *MNRAS*, 398, 1150
- Chandrasekhar, S. 1943, *ApJ*, 97, 255
- Ciardi, B. Ferrara, A. 2005, *SSR*, 116, 625
- Colpi, M., Mayer, L., Governato, F. 1999, *ApJ*, 525, 720
- Crocce, M., Pueblas, S., Scoccimarro, R. 2006, *MNRAS*, 373, 369
- Croton, D. J., et al. 2006, *MNRAS*, 365, 11
- Fujii, M., Funato, Y., Makino, J. 2006, *PASJ*, 58, 743
- Han, J., Jing, Y. P., Wang, H., Wang, W. 2011, *ArXiv e-prints*
- Hashimoto, Y., Funato, Y., Makino, J. 2003, *ApJ*, 582, 196
- Jiang, C. Y., Jing, Y. P., Faltenbacher, A., Lin, W. P., Li, C. 2008, *ApJ*, 675, 1095
- Jiang, C. Y., Jing, Y. P., Lin, W. P. 2010, *A&A*, 510, A60
- Kauffmann, G., White, S. D. M., Guiderdoni, B. 1993, *MNRAS*, 264, 201
- Klypin, A., Gottlöber, S., Kravtsov, A. V., Khokhlov, A. M. 1999, *ApJ*, 516, 530
- Lacey, C. Cole, S. 1993, *MNRAS*, 262, 627
- Lin, D. N. C. Tremaine, S. 1983, *ApJ*, 264, 364
- Ludlow, A. D., Navarro, J. F., Springel, V., Jenkins, A., Frenk, C. S., Helmi, A. 2009, *ApJ*, 692, 931
- Micic, M., Holley-Bockelmann, K., Sigurdsson, S. 2011, *MNRAS*, 414, 1127
- Micic, M., Holley-Bockelmann, K., Sigurdsson, S., Abel, T. 2007, *MNRAS*, 380, 1533
- Navarro, J. F., Frenk, C. S., White, S. D. M. 1995, *MNRAS*, 275, 56
- Power, C., Navarro, J. F., Jenkins, A., Frenk, C. S., White, S. D. M., Springel, V., Stadel, J., Quinn, T. 2003, *MNRAS*, 338, 14
- Rubin, V. C., Ford, W. K. J., Thonnard, N. 1980, *ApJ*, 238, 471
- Sales, L. V., Navarro, J. F., Abadi, M. G., Steinmetz, M. 2007, *MNRAS*, 379, 1475
- Sinha, M. Holley-Bockelmann, K. 2012, *ApJ*, 751, 17
- Somerville, R. S., Hopkins, P. F., Cox, T. J., Robertson, B. E., Hernquist, L. 2008, *MNRAS*, 391, 481
- Spergel, D. N., et al. 2007, *ApJS*, 170, 377
- Springel, V. 2005, *MNRAS*, 364, 1105
- Springel, V., White, S. D. M., Tormen, G., Kauffmann, G. 2001, *MNRAS*, 328, 726
- Taylor, J. E. Babul, A. 2001, *ApJ*, 559, 716
- Tormen, G., Diaferio, A., Syer, D. 1998, *MNRAS*, 299, 728
- Tremaine, S. Weinberg, M. D. 1984, *MNRAS*, 209, 729
- Tremaine, S. D., Ostriker, J. P., Spitzer, Jr., L. 1975, *ApJ*, 196, 407
- van den Bosch, F. C., Lewis, G. F., Lake, G., Stadel, J. 1999, *ApJ*, 515, 50
- Volonteri, M., Haardt, F., Madau, P. 2003, *ApJ*, 582, 559
- Weinberg, M. D. 1989, *MNRAS*, 239, 549
- Wetzel, A. R. 2011, *MNRAS*, 412, 49
- Wetzel, A. R. White, M. 2010, *MNRAS*, 403, 1072
- White, S. D. M. 1976, *MNRAS*, 174, 467
- Zel'Dovich, Y. B. 1970, *A&A*, 5, 84
- Zwicky, F. 1933, *Helvetica Physica Acta*, 6, 110

## 6 APPENDIX

### 6.1 Details of our Merger-tree

Sinha & Holley-Bockelmann (2012) try to quantify the effect of flybys for corrections in current models. To address this issue and avoid “false mergers” in the current work we apply the following conditions in the construction of our merger-trees.

- Any halo associated with the tree has at least 50% of its particles in the “root” halo at  $z=0$ .
- If there is any ambiguity as to which halo is the main progenitor (in snap i-1), we then follow the contributions of the both progenitors back to i-10.
- One of the benefits of P-groupfinder is that particle ids in a given halo are listed in order of binding energy (to a large extent although not exactly<sup>6</sup>) this allow us to weight the mutual particles such that more bound particles hold greater weight when considering progenitors (Boylan-Kolchin et al. 2009).
- When a halo in snapshot i traces to a significantly larger halo in snapshot i-1 (i.e an emerging flyby), we look at snapshots i-10 through to i+10 to firstly establish what the halos mass was upon in-fall and secondly to see whether the halo grows significantly after it emerges. To distinguish between flybys and highly eccentric orbits we employ the condition that a satellite must at least double its initial in-fall mass to be considered independent after emergence (Wetzel 2011).

While these approaches help to minimize the number of flybys it does not catch all of them. A small fraction of mergers are false mergers due to flybys. These mergers are removed from further kinematic analysis. Figure 8 shows an example merger-tree.

### 6.2 Our Tracking Scheme: The Importance of a Fixed Particle Set

An initial attempt to track mergers by comparing substructure at different snapshots (via common particle ids) proved difficult due to the limitations of single epoch group-finders.

<sup>6</sup> P-groupfinder lists the particles in order of binding energy for each substructure. It lists the substructure in a given halo from largest to smallest.

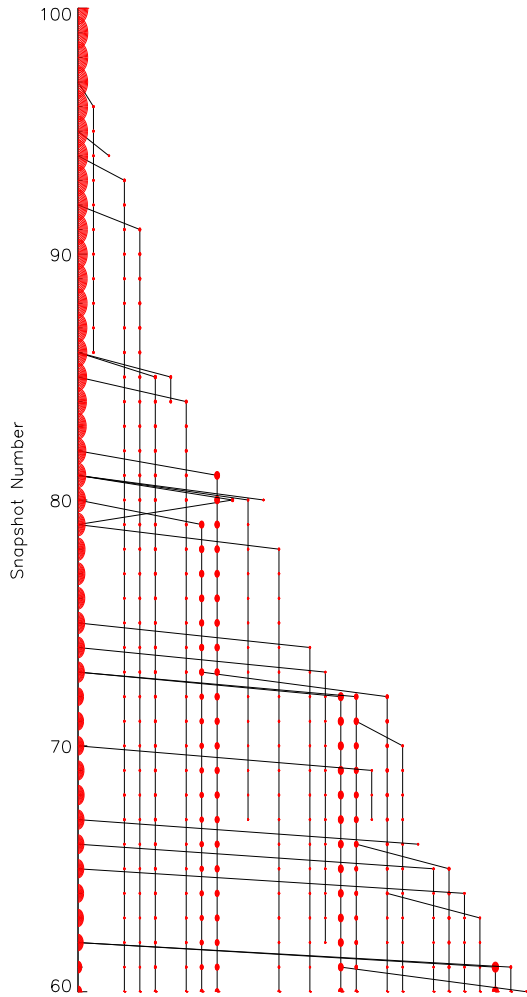


**Figure 8.** An example of one of our merger-trees. The size of the circles is proportional to the size of the halo.

Subfind identifies substructure by constructing a smoothed 3D density contour of the FOF halo. As the global density is lowered, saddle points emerge between adjacent over-densities (Springel et al. 2001). This gives a subset of particles that Poisson’s equation can be applied to.

Subfind can temporarily lose substructure when the subhalo is passing through an over-dense region. The cause of this intermittent loss arises from the position based (i.e. smoothed density) selection of particles. It is important to track all particles associated with the satellite halo at in-fall when measuring the evolution of satellite properties.

Figure 9 shows a 2D projection of structure found by various methods at three points during the merger. The first two columns show the subfind substructure (blue) compared with the satellite tracing scheme used in this work (green). It is important to highlight that the blue particles correspond to *all* substructure in the FOF halo and the plots in each row are centred on the same coordinates. The middle row ( $z=2.22$ ) shows the substructure found as the satellite passes through a region of high background density.

The third column of figure 9 has a different scale to the first two in order to highlight the bound particles in reference to their unbound counterparts. This demonstrates the effectiveness of our tracking scheme above and beyond the groupfinder-particle tracking approach. See Han et al. (2011) for a more detailed comparison.

XY plots of a satellite halo during merger

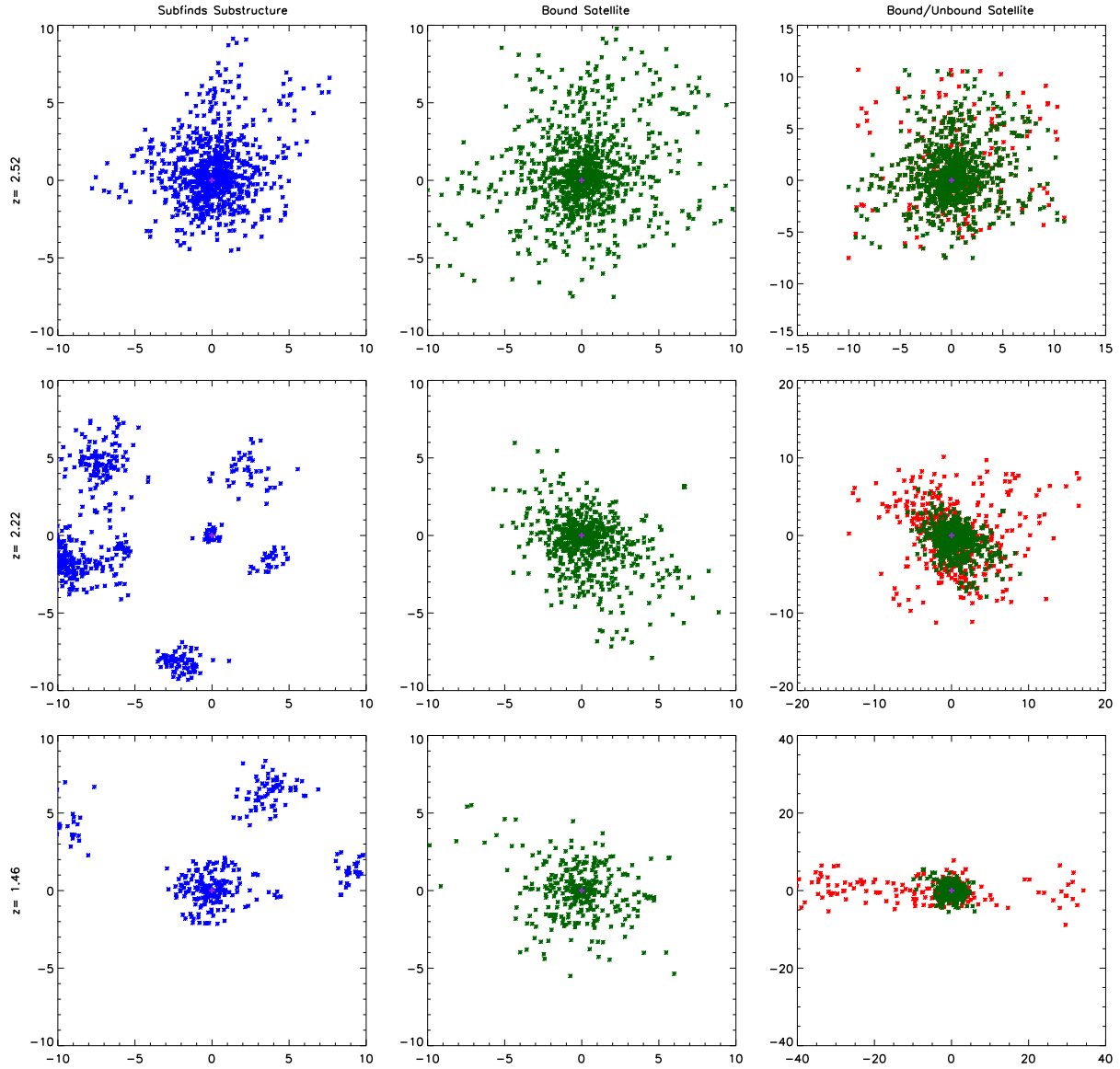


**Figure 9.** A 2D comparison of the structure found with subfind at 3 points during a merger. The first two columns show the subfind substructure (blue) compared with the satellite tracing scheme used in this work (green). The final column shows the bound(green) to unbound (red) particles of the satellite in the broader context of tidal stripping. **Note that column 3 has a different and varying distance scale to the first two columns.** All columns are centred on the same coordinates.